AGGREGATE INTERFERENCE MODELING IN COGNITIVE RADIO NETWORKS WITH POWER AND CONTENTION CONTROL

Zengmao Chen[1], Cheng-Xiang Wang[1], Xuemin Hong[2], John Thompson[3]
Sergiy A. Vorobyov[4], Xiaohu Ge[5], Hailin Xiao[6], and Feng Zhao[7]

[1] Joint Research Institute for Signal and Image Processing
School of Engineering & Physical Sciences
Heriot-Watt University, Edinburgh, EH14 4AS, UK.
Email:{zengmao.chen, cheng-xiang.wang}@hw.ac.uk

[2]School of Information Science and Technology
Xiamen University, Xiamen 361005, China.
Email: xuemin.hong@xmu.edu.cn

[3]Joint Research Institute for Signal and Image Processing
Institute for Digital Communications
University of Edinburgh,Edinburgh, EH9 3JL, UK.
Email: john.thompson@ed.ac.uk

[4] Department of Electrical and Computer Engineering
University of Alberta, Edmonton, AB, T6G 2V4, Canada.
Email: vorobyov@ece.ualberta.ca

[5]Department of Electronics and Information Engineering
Huazhong University of Science and Technology, Wuhan 430074, China.
Email: xhge@mail.hust.edu.cn

[6]School of Information and Communication
Guilin University of Electronic Technology, Guilin 541004, China.
Email: xhl_xiaohailin@yahoo.com.cn

[7]Department of Science and Technology
Guilin University of Electronic Technology, Guilin 541004, China.
Email: zhaofeng@guet.edu.cn

Abstract

In this paper, we present interference models for cognitive radio (CR) networks employing various interference management mechanisms including power control, contention control or hybrid power/contention control schemes. For the first case, a power control scheme is proposed to govern the transmission power of a CR node. For the second one, a contention control scheme at the media access control (MAC) layer, based on carrier sense multiple access with collision avoidance (CSMA/CA), is proposed to coordinate the operation of CR nodes with transmission requests. The probability density functions (PDFs) of the interference received at a primary receiver from a CR network are first derived numerically for these two cases. For the hybrid case, where power and contention controls are jointly adopted by a CR node to govern its transmission, the interference is analysed and compared with that of the first two schemes by simulations. Then, the interference PDFs under the first two control schemes are fitted by log-normal PDFs to reduce computation complexity. Moreover, the effect of a hidden primary receiver on the interference experienced at the receiver is investigated. It is demonstrated that both power and contention controls are effective approaches to alleviate the interference caused by CR networks. Some in-depth analysis of the impact of key parameters on the interference of CR networks is given as well.

Index Terms – Cognitive radio, interference modeling, power control, contention control, hidden primary receiver.

I. INTRODUCTION

With the requirement to improve spectrum utilisation, the newly emerging cognitive radio (CR) technology [1]– [4] has attracted increasing attention. A CR network is envisioned to be capable of reusing the unused or underutilised spectra of incumbent systems (also known as primary networks) by sensing its surrounding environment and adapting its operational parameters autonomously. A CR system may coexist with a primary network on either an interference-free or interference-tolerant basis [5]. For the former case, the CR system only exploits the unused spectra of the primary network, which consequently guarantees no interference to primary users. For the latter case, the CR system is allowed to share the spectra assigned to the primary network, under the condition that the CR network must not impose detrimental interference on the primary network. Therefore, modeling and analysing the interference caused by CR networks is of great importance to reveal how the service of a primary network is deteriorated and how CR networks may be deployed to protect the primary network against detrimental interference.

In the literature, the existing research on interference modeling for CR networks mainly falls into three categories: spatial, frequency-domain and accumulated interference modeling. For spatial interference modeling, the fraction of white spaces available for CR networks was investigated in [6] and [7]. In [8], the region of interference for CR receivers and region of communication for CR transmitters were studied for the case where a CR network coexists with a cellular network. The interference from CR devices to wireless microphones operating in TV bands was analysed in [9], where the loss of reliable communication area of a wireless microphone due to the existence of CR devices was examined. CR interference in the frequency domain was also researched in the literature, e.g., the interference due to out-of-band emission of a wireless regional area network (WRAN) was analysed in [10].

As for accumulated interference modeling, in [11], the aggregate interference power from a sea of CR transmitters surrounding a primary receiver was derived. The performance of a primary system was evaluated in [12] in terms of outage probability caused by the interference from CR networks. The outage probability was derived for both underlay and overlay spectrum sharing cases. In [13] the aggregate interference from multiple CR transmitters following a Poisson point process was approximated by a Gamma distribution and the probability of interference at a primary receiver was also given. It is worth noting that only pathloss was assumed for the interfering channel in [11]– [13]. Their work was extended by taking both shadowing and fading

into account in [14] and [15]. Moreover, the probability density function (PDF) for accumulated interference and outage probability due to the aggregate interference from CR nodes were also derived in [14] and [15], respectively.

However, in all the previous works [6]– [15], the CR transmitters were assumed to transmit at a fixed power level. Moreover, the CR nodes were all assumed to communicate with each other simultaneously. Thus, no contention control scheme was employed at the cognitive media access control (MAC) layer. In [16], some preliminary interference modeling was reported by considering power and contention control schemes. In this paper, we present more realistic and comprehensive interference models by significantly extending the work of [16]. Firstly, a more realistic power control scheme than that in [16] is proposed, and a new interference management scheme - hybrid power/contention control scheme is introduced. Secondly, the PDFs of interference perceived at a primary network from a CR network are derived numerically for the cases of power or contention control. The interference distribution of the hybrid control scheme is also analysed and compared with that of the pure power control and pure contention control schemes by simulations. Furthermore, to reduce the complexity of the numerical interference PDF's computation used in [16], cumulant-based approximations are applied to fitting the interference distributions. Finally, the impact of a hidden primary receiver on the aggregate interference is also investigated. The interference modeling presented in this work considers several basic interference management schemes, which forms a fundamental basis for the development of other advanced interference models for CR networks. Secondly, it gives insights into CR deployment by figuring out how to optimise CR operation parameters. Finally, the interference modeling lays a foundation for performance evaluation of primary networks, e.g., outage capacity of primary systems can be derived based on the interference PDFs.

The remainder of this paper is organised as follows. The system model is elaborated in Section II. The detailed interference modeling is presented in Section III. In Section IV, the interference distributions are approximated by log-normal distributions. We incorporate the hidden primary receiver problem in Section V. The impact of several key parameters on the interference is analysed via numerical studies in Section VI. Finally, Section VII concludes the paper.

II. System Model

The system model is illustrated in Fig. 1. It consists of a CR network coexisting with a primary transmitter-receiver pair. The *interference region* (IR) is adopted by the primary network

to protect itself against interference from the CR network. No CR transmission is allowed within the IR. There exist two main types of techniques to identify the IR for a primary network: geo-location technique and spectrum sensing [17]. For geo-location-based CR networks, the global positioning system (GPS) can be incorporated within the CR network. It enables CR transmitters to determine whether they are located far enough outside the protected service contour of the primary system. The geo-location technology usually leads to a circular IR around the primary system. As for spectrum-sensing-based CR, the IR is usually not circular but more irregular than that of the geo-location-based CR due to fading and/or imperfect sensing. In this paper, we focus on the former type and thus, a circular IR with a radius R is considered.

The underlying interference channels from CR transmitters to the primary receiver experience pathloss, shadowing and fading. The pathloss function $g(r_j)$ is

$$g(r_j) = r_j^{-\beta} \tag{1}$$

where r_j is the distance between the jth $(j = 1, 2, \cdots)$ active CR transmitter and the primary receiver and β is the pathloss exponent. The composite model for shadowing and fading can be expressed as the product of the long term shadowing and the short term multipath fading. In this paper, log-normal shadowing and Nakagami fading are considered. Let h_j denote the channel gain for the composite shadowing and fading of the interference channel from the jth active CR transmitter to the primary receiver. The PDF of the composite channel gain h_j can be approximated by the following log-normal distribution [18] (Page 102)

$$f_{\mathrm{h}}(x) \approx \frac{1}{\sqrt{2\pi}\sigma x} \exp\left\{-\frac{(\ln(x)-\mu)^2}{2\sigma^2}\right\} \tag{2}$$

where the mean μ and variance σ^2 can be expressed as

$$\mu = \left(\sum_{k=1}^{m-1}\frac{1}{k} - \ln(m) - 0.5772\right) + \mu_\Omega \tag{3}$$

$$\sigma^2 = \sum_{k=0}^{\infty}\frac{1}{(m+k)^2} + \sigma_\Omega^2 \tag{4}$$

with m standing for the Nakagami shape factor and μ_Ω and σ_Ω^2 denoting the standard mean and variance of the log-normal distribution, respectively.

Let p_j denote the transmission power of the jth active CR transmitter. The accumulated power of the instantaneous interference received at the primary receiver can be expressed as

$$Y = \sum_{j=1}^{\infty} p_j g(r_j) h_j. \tag{5}$$

In this paper, we investigate the characteristics of the aggregate interference from all CR transmitters employing the following three different interference management schemes: (i) power control, (ii) contention control, and (iii) hybrid power/contention control.

A. Power Control

In this scenario, the distribution of active CR transmitters follows a Poisson point process with a density parameter λ for the density of CR transmitters on the plane.

The transmission power of a CR transmitter is governed by the following power control law

$$p_{\mathrm{pwc}}(r_{\mathrm{cc}_j}) = \begin{cases} \left(\frac{r_{\mathrm{cc}_j}}{r_{\mathrm{pwc}}}\right)^{\alpha} P_{\max}, & 0 < r_{\mathrm{cc}_j} \leq r_{\mathrm{pwc}} \\ P_{\max}, & r_{\mathrm{cc}_j} > r_{\mathrm{pwc}} \end{cases} \tag{6}$$

where r_{cc_j} is the distance from the jth active CR transmitter to its nearest neighbouring active CR transmitter, α is the power control exponent, $P_{\max}$ is the maximum transmission power for CR transmitters, and r_{pwc} is the power control range, which determines the minimum r_{cc_j} leading to maximum CR transmission power $P_{\max}$. Compared to the power control law in [16], a new parameter r_{pwc} is introduced here to adjust the range of the power control. The interference caused by the jth active CR transmitter to its nearest active CR transmitter due to pathloss is $p_{\mathrm{pwc}}(r_{\mathrm{cc}_j})g(r_{\mathrm{cc}_j})$. The above proposed power control scheme is designed in such a manner that when $\alpha = \beta$ within the power control range r_{pwc}, this interference is equal to a constant $P_{\max}/r_{\mathrm{pwc}}^{\alpha}$. Beyond the power control range, the interference is smaller than that constant. This means that at any CR transmitter, the interference from the nearest neighbouring CR transmitter is capped and independent of the nearest neighbour distance within the power control range.

A CR network can be deployed as either an infrastructure or an ad hoc network [2]. For a CR infrastructure network, the above power control scheme is applicable to CR base stations (BSs), whose transmission powers are usually determined by their coverages. Moreover, the CR BSs locations are usually fixed, which minimises the network planning load to determine the transmission power of CR BSs. When CR BSs follow a Poisson point distribution, the PDF of r_{cc_j} can be given as [20]

$$f_{\mathrm{cc}}(x) = 2\pi\lambda x e^{-\lambda\pi x^2}. \tag{7}$$

B. Contention Control

Unlike the abovementioned power control scheme, for the case of contention control every active CR transmitter has fixed transmission power p, but their transmission is governed by contention control to determine which CR transmitters can transmit at a given time. We assume that

the multiple access protocol carrier sense multiple access with collision avoidance (CSMA/CA) is employed, like in IEEE 802.11 networks. Every CR transmitter senses the medium before transmission. If the medium is busy, namely, the CR transmitter detects transmission from other CR transmitters within its contention region, it defers its transmission. Otherwise, the CR transmitter starts its transmission. As a result of the contention control, all the active CR transmitters are separated from each other by at least the contention distance, which is the minimum distance $d_{\min}$ between two concurrent CR transmitters. The contention control scheme can be applied to either a CR ad hoc network or distributed multiple-access users of a CR infrastructure network.

The distribution of active CR transmitters under the contention control scheme can be modeled as a Matern-hardcore (MH) point process [19]. The MH point process $\Phi_{\rm mh}$ can be obtained by thinning a Poisson point process Φ, which can be expressed as follows [20]

$$\Phi_{\rm mh} = \{x \in \Phi \mid m(x) < m(y) \text{ for all } y \text{ in } \Phi \cap C(x, d_{\min})\}. \tag{8}$$

Each point x in the original Poisson point process Φ is marked with a random variable $m(x)$ uniformly distributed in $(0, 1)$. A point x is retained from the thinning process only if its mark is smaller than that of all the other points within the disk $C(x, d_{\min})$ centered at point x with the radius $d_{\min}$. Otherwise, the point x is removed. The *retaining probability* $q_{\rm mh}$ for the MH point process, which is the probability of a point from a Poisson point process with a density λ surviving the thinning process, is given by [20]

$$q_{\rm mh} = \frac{1 - e^{-\lambda\pi d_{\min}^2}}{\lambda\pi d_{\min}^2}. \tag{9}$$

C. Hybrid Power/Contention Control

A natural extension of the above two interference management schemes is to implement both schemes in the same system. This is termed hybrid power/contention control and it works in the following manner. The contention control scheme is first applied, resulting in a set of active CR transmitters following an MH point process. Then, a power control scheme similar to (6) is employed to adjust the transmission power of each active CR transmitter according to the distance to the nearest neighbouring active transmitter. The following power control law is adopted in the hybrid control scheme

$$p_{\rm hyb}(r) = \begin{cases} \left(\frac{r_{cc}}{d_{\min}}\right)^{\alpha} p, & d_{\min} \leq_{cc} \leq r_{\rm hyb} \\ \left(\frac{r_{\rm hyb}}{d_{\min}}\right)^{\alpha} p, & _{cc} > r_{\rm hyb} \end{cases} \tag{10}$$

where r_{cc} is the distance from an active CR transmitter to its nearest neighbouring active CR transmitter, α is the power control exponent as in (6), and $r_{\rm hyb}$ is the power control range similar to $r_{\rm pwc}$ in (6) except that it also determines the maximum transmission power, i.e., $\left(\frac{r_{\rm hyb}}{d_{\min}}\right)^{\alpha} p$. The above power control law (10) guarantees that when a pathloss channel is considered for each active CR transmitter, the perceived interference caused by its nearest neighbouring CR transmitter is $p_{\rm hyb}(r_{cc})g(r_{cc})$, which is (i) a constant $p/d_{\min}^{\alpha}$ (if $\alpha = \beta$) within the power control range $r_{\rm hyb}$ and (ii) less than the constant when r is larger than the power control range.

III. Interference Modeling

We intend to model the aggregate interference from CR transmitters employing the three different interference management schemes introduced in Section II by finding their corresponding PDFs. We apply the characteristic-function-based method used, for example, in [14] and [21] to derive the PDFs. First, the characteristic functions of the interference under different system models are derived. Then, the PDFs of the aggregate interference are obtained by performing an inverse Fourier transform on their characteristic functions.

A. Power Control

When all the CR transmitters follow a Poisson point process distribution and employ the power control scheme proposed in (6), we can adopt the characteristic function-based method as in [14], [21]- [23] and obtain the following characteristic function $\phi_{\rm Y}(\omega)$ of the aggregate interference Y at a primary receiver from all CR transmitters

$$\phi_{\rm Y}(\omega) = \exp\left(\lambda\pi \int_H f_{\rm h}(h) \int_P f_{\rm p}(p) T(\omega p h) dp\ dh\right) \tag{11}$$

where $f_{\rm p}(\cdot)$ is the PDF of the CR transmission power $p_{\rm pwc}(r_{{\rm cc}_j})$ defined in (6) and

$$T(\omega p h) = R^2(1 - e^{i\omega g(R) p h}) + i\omega p h \int_0^{g(R)} [g^{-1}(t)]^2 e^{i\omega t p h} dt. \tag{12}$$

In (12), $g^{-1}(\cdot)$ denotes the inverse function of $g(\cdot)$ in (1). For the derivation of (11), the following fact is used: the distance from a CR transmitter to the primary receiver r has independent and identical uniform distributions for a given number of CR transmitters [21]. Their PDFs have the following form [21]

$$f_{\rm r}(r) = \begin{cases} 2r/(l^2 - R^2), & R \le r \le l \\ 0, & \text{otherwise} \end{cases} \tag{13}$$

when CR transmitters are distributed within an annular ring with inner radius R and outer radius l. In (11), p is a function of $r_{\rm cc}$ as shown in (6), so the expectation of $T(\omega ph)$ over p equals that of $T(\omega p_{\rm pwc}(r_{\rm cc})h)$ over $r_{\rm cc}$. Using the PDF of $r_{\rm cc}$ given in (7), (11) can be rewritten as

$$\phi_{\rm Y}(\omega) = \exp\left(\lambda\pi \int_H f_{\rm h}(h) \int_{r_{\rm cc}} f_{\rm cc}(x) T(\omega p_{\rm pwc}(r_{\rm cc})h) dx dh\right). \tag{14}$$

Moreover, (14) can be written as (see Appendix A for the detailed derivation procedure)

$$\begin{aligned}\phi_{\rm Y}(\omega) = \exp\Bigg\{\lambda\pi\int_H f_{\rm h}(h)\int_0^{r_{\rm pwc}} f_{\rm cc}(x)\Bigg[R^2\Bigg(1-e^{\frac{i\omega x^\alpha P_{\max} g(R) h}{{r_{\rm pwc}}^\alpha}}\Bigg) \\ + \frac{i\omega x^\alpha P_{\max} h}{{r_{\rm pwc}}^\alpha}\int_0^{g(R)} t^{-\frac{2}{\beta}} e^{\frac{i\omega t x^\alpha P_{\max} h}{{r_{\rm pwc}}^\alpha}} dt\Bigg] dx dh \\ +\lambda\pi\int_H f_{\rm h}(h)\int_{r_{\rm pwc}}^{\infty} f_{\rm cc}(x)\Bigg[R^2\big(1-e^{i\omega g(R) P_{\max} h}\big) + i\omega P_{\max} h\int_0^{g(R)} t^{-\frac{2}{\beta}} e^{i\omega t P_{\max} h} dt\Bigg] dx dh\Bigg\}.\end{aligned} \tag{15}$$

Finally, we obtain the PDF of the interference by performing the inverse Fourier transform on $\phi_{\rm Y}(\omega)$ as

$$f_{\rm Y}(y) = \frac{1}{2\pi}\int_{-\infty}^{+\infty} \phi_{\rm Y}(\omega) e^{-2\pi i\omega y} d\omega. \tag{16}$$

B. Contention Control

As mentioned in Section II.B, the distribution of CR transmitters can be modeled as an MH point process when the contention control is adopted. However, the thinning process depicted in (8) does not consider the existence of the IR. For CR transmitters right outside of the IR, their retaining probability and also the density of the MH process are affected by the IR. More specifically, for a CR transmitter with $R < r < R + d_{\min}$ whose contention region intersects with the IR as shown in Fig. 2, its retaining probability and hence the density of retained CR transmitters is determined by the dotted region $\mathscr{A}$ shown in Fig. 2. After some algebraic manipulations, we obtain the area A of the dotted region as follows

$$A = R^2(\gamma - \sin\gamma\cos\gamma) + d_{\min}^2(\eta - \sin\eta\cos\eta) \tag{17}$$

where

$$\gamma = \arccos\frac{R^2 + r^2 - d_{\min}^2}{2Rr} \tag{18}$$

$$\eta = \arccos\frac{r^2 + d_{\min}^2 - R^2}{2rd_{\min}}. \tag{19}$$

The density of active CR transmitters by adopting the contention control scheme can be expressed as

$$\lambda_{\rm cnt}(r) = \begin{cases} \lambda_{\rm mh} = \lambda q_{\rm mh} = \frac{1-e^{-\lambda\pi d_{\min}^2}}{\pi d_{\min}^2}, & r \geq R + d_{\min} \\ \lambda_{\rm roIR}(r) = \frac{1-e^{-\lambda(\pi d_{\min}^2 - A)}}{\pi d_{\min}^2 - A}, & R < r < R + d_{\min} \\ 0, & \text{otherwise} \end{cases} \tag{20}$$

where $\lambda_{\rm roIR}(r)$ denotes the density of active CR transmitters right outside of the IR with $R < r < R + d_{\min}$. It can be proved that $\lambda_{\rm roIR}(r)$ is a monotonically decreasing function of r with $\lambda_{\rm roIR}(R + d_{\min}) = \lambda_{\rm mh}$.

For active CR transmitters located in the region $r \geq R + d_{\min}$, the distribution of their aggregate interference is equivalent to that of a Poisson point process with density $\lambda_{\rm mh}$. This is due to the fact that the thinning process (8) is independent of r in this region. Therefore, the active CR transmitters in this region have a uniformly distributed value of r similar to (13) given a total number of active CR transmitters. While, for active CR transmitters located right outside of the IR with $R < r < R + d_{\min}$, the characteristic function of the aggregate interference analogous to (11) is difficult to obtain due to the fact that $\lambda_{\rm roIR}(r)$ is not fixed like $\lambda_{\rm mh}$, but changes over r. To model the distribution of the aggregate CR interference under the contention control scheme, we can approximate the thinning process by ignoring the impact of the IR. The approximated density of active CR transmitters can be written as follows

$$\lambda_{\rm apprx} = \begin{cases} \lambda_{\rm mh}, & r > R \\ 0, & \text{otherwise} \end{cases} \tag{21}$$

To this end, the aggregate CR interference distribution under contention control can be approximated by that of a Poisson point process with density $\lambda_{\rm mh}$ and fixed transmission power p. The characteristic function of the accumulated interference can be found as

$$\phi_{\rm Y}(\omega) = \exp\left(\lambda_{\rm mh}\pi \int_H f_{\rm h}(h) T(\omega p h) dh\right). \tag{22}$$

The detailed derivation of (22) is presented in Appendix B.

By comparing (20) and (21), one can find out that the approximated thinning process underestimates the aggregate CR interference due to the monotonically decreasing nature of $\lambda_{\rm roIR}(r)$. Some active CR transmitters located in the region $R < r < R + d_{\min}$ are ignored during the approximation, i.e., the approximated distribution (22) serves as a lower bound for the CR interference distribution under the contention control scheme. The accuracy of the above

approximation depends on the difference between $\lambda_{\mathrm{roIR}}(r)$ and λ_{mh}. It can be seen from (17)–(20) that $\lambda_{\mathrm{roIR}}(r)$ is determined by λ, $d_{\min}$ and R. In Fig. 3, we evaluate the impact of these parameters on the ratio $\lambda_{\mathrm{roIR}}(R)/\lambda_{\mathrm{mh}}$, which relates to the accuracy of the approximation. It is easy to understand that the approximation becomes more accurate as the ratio $\lambda_{\mathrm{roIR}}(R)/\lambda_{\mathrm{mh}}$ decreases and approaches 1. By observing Fig. 3, the following points may be observed: (i) the approximation tends to be less accurate as the density λ and/or IR radius R increase; (ii) for small λ, the approximation accuracy is inversely proportional to $d_{\min}$; while, for large λ, the accuracy is proportional to $d_{\min}$; (iii) the density λ has less influence on the approximation accuracy as it increases, since the ratio saturates. The approximation accuracy is evaluated numerically in Section IV.B as well.

C. Hybrid Power/Contention Control

To model the aggregate interference under the hybrid control scheme, the nearest neighbouring distance distribution function analogous to (7) for active CR transmitters is indispensable to evaluate the transmission power designated in (10). Unfortunately, there is no closed-form expression for the nearest neighbour distance distribution function for an MH point process [24]. Thus, we approach this problem numerically.

The PDF for the aggregate interference under the hybrid control scheme is simulated in Fig. 4, where the interference PDFs for power and contention control are given as well for the purpose of comparison. It can be seen from this figure that with the setup of $d_{\min} = r_{\mathrm{pwc}}$, $p = P_{\max}$ and $\alpha = \beta$ both the mean and variance of the aggregate interference increase for the hybrid control scheme compared to either power or contention control schemes. However, the boosted interference is paid off by the increased CR communication area (coverage) for the hybrid control scheme. We define the coverage of each CR transmitter as a circular disk centered at a CR transmitter with radii being $\min(r/2, r_{\mathrm{pwc}}/2)$, $d_{\min}/2$ and $\min(r/2, r_{\mathrm{hyb}}/2)$ for power control, contention control and hybrid power/contention control schemes, respectively. Then, the received signal power at cell edge of a CR transmitter due to pathloss is $2^{\beta}P_{\max}/{r_{\mathrm{pwc}}}^{\beta}$, $2^{\beta}p/d_{\min}^{\beta}$ and $2^{\beta}p/d_{\min}^{\beta}$, which is same for all the three schemes under the aforementioned setup. With this setup, the overall coverage ratio obtained numerically among the power, contention and hybrid power/contention control is $1.0093 : 1 : 2.0229$. Two interesting facts are unveiled from this experiment. Firstly, with the setup of $d_{\min} = r_{\mathrm{pwc}}$, $p = P_{\max}$ and $\alpha = \beta$, the power and contention control schemes lead to almost the same amount of interference and coverage, but

the latter is less complex to implement. Secondly, introducing power control into the contention control scheme can enlarge the coverage compared to the pure contention control scheme at the cost of causing higher interference to the primary system.

IV. Analytical Approximation

In the previous section, to derive the PDFs for aggregate interference, the characteristic function-based method has been used which consists of two steps. Namely, characteristic function computation and Fourier transformation. This interference modeling approach is extremely computation-intensive, since generally closed-form expressions are not admitted for either step and the computations in both steps have to be performed numerically. It is desirable to model the aggregate interference with less complexity. An alternative approach to model the interference, which greatly reduces complexity, is to approximate interference PDFs as certain known distributions. Observations from Fig. 4 suggest that the interference distribution for either power or contention control is positively skewed and heavy-tailed, which suggests a log-normal distribution. Thus, in this section, we fit the aggregate interference under power and contention control schemes to log-normal distributions. The theory behind the log-normal fitting is based on the following two facts. It has been shown that the sum of interference from uniformly distributed interferers in a circular area is asymptotically log-normal [15], [25]. This ensures that the aggregate interference in these two schemes can be approximated as log-normal distributed. Meanwhile, the sum of randomly weighted log-normal variables can be modelled as a log-normal distribution as well [26], which guarantees that the aggregate interference is still log-normal distributed even if the effect of shadow fading (2) is taken into account. In what follows, the log-normal fitting is performed using a cumulant-matching approach [27], where the first two order cumulants of the aggregate interference Y in (5) are used to estimate the mean and variance of the log-normal distribution function. Therefore, the exact PDFs of interference can be obtained. Fortunately, these cumulants have closed-form expressions for both control schemes. Consequently, it significantly reduces the complexity compared to the interference modeling carried out in Section III. Moreover, compared to the characteristic function-based method, the relationship between CR system parameters and the resulting interference becomes much clearer for the cumulant-based PDFs approximation.

For a log-normal random variable, its mean μ and variance σ^2 can be estimated using the first

two order cumulants k_1 and k_2 as follows [28]:

$$\mu = \ln \frac{k_1}{\sqrt{\frac{k_2}{k_1^2}+1}} \tag{23}$$

$$\sigma^2 = \ln\left(\frac{k_2}{k_1^2}+1\right). \tag{24}$$

In the context of interference distribution fitting, the nth cumulant k_n of the aggregate interference Y can be obtained from its characteristic function $\phi_{\rm Y}(\omega)$ via the following equation

$$k_n = \frac{1}{i^n}\left[\frac{\partial^n \ln\phi_{\rm Y}(\omega)}{\partial\omega^n}\right]_{\omega=0}. \tag{25}$$

A. Power Control

From (15) and (25), the cumulants for aggregate interference under the power control scheme can be derived as (see Appendix C for detailed derivation)

$$k_n = \frac{2\lambda\pi P_{\max}^n e^{n\mu+\frac{n^2\sigma^2}{2}}}{(n\beta-2)R^{n\beta-2}}\left[\frac{n\alpha(n\alpha-2)\cdots 2}{{r_{\rm pwc}}^{n\alpha}(2\pi\lambda)^{\frac{n\alpha}{2}}}\left(1-e^{-\lambda\pi {r_{\rm pwc}}^2}\right)\right.$$
$$\left. -\sum_{i=1}^{\frac{n\alpha}{2}-1}\frac{n\alpha(n\alpha-2)\cdots(n\alpha-2i+2)}{(2\pi\lambda {r_{\rm pwc}}^2)^i}{r_{\rm pwc}}^{n\alpha-2i}e^{-\lambda\pi {r_{\rm pwc}}^2}\right]. \tag{26}$$

It can be seen from (26) that k_n is proportional to $P_{\max}^n$ and $1/R^{n\beta-2}$, and all cumulants are most sensitive to the IR radius R since it has the highest exponent compared to other parameters. The power control range $r_{\rm pwc}$ and the density λ have similar impact on all cumulants, but the impact of the former is larger than that of the latter, since the former has a larger exponent.

To evaluate the accuracy of the approximation for the power control case, comparisons are performed in Fig. 5(a), where cumulative distribution functions (CDFs) are used to improve readability. It can be seen from Fig. 5(a) that there is fairly good agreement among the interference CDFs derived in Section III, the approximated counterparts and the Monte Carlo simulation. This approximation approach can be applied to both the pathloss-only and shadow fading channels.

B. Contention Control

Following the similar steps as in Appendix C and given the characteristic function (22) for the aggregate interference under contention control and also using (25), we can find the nth

cumulant k_n of aggregate interference as

$$\begin{aligned} k_n &= \frac{\lambda\pi q_{\mathrm{mh}}}{i^n}\int_H f_{\mathrm{h}}(h)\left[-R^2\left(ipg(R)h\right)^n + n\left(iph\right)^n\int_0^{g(R)} t^{n-1-\frac{2}{\beta}}dt\right]dh \\ &= \lambda\pi q_{\mathrm{mh}}\left(\frac{n}{n-\frac{2}{\beta}}g^{n-\frac{2}{\beta}}(R) - R^2 g^n(R)\right)p^n\int_H f_{\mathrm{h}}(h)h^n dh \\ &= \frac{2p^n\left(1-e^{-\lambda\pi d_{\min}^2}\right)e^{n\mu+\frac{n^2\sigma^2}{2}}}{(n\beta-2)d_{\min}^2 R^{n\beta-2}}. \end{aligned} \tag{27}$$

As we can see from (27), k_n is linear to p^n and $1/R^{n\beta-2}$, which suggests that IR radius R is the most effective parameter to control the aggregate interference due to its highest exponent. The cumulants are not sensitive to the CR density λ for large λ. The contention range $d_{\min}$ has little impact on the cumulants when $d_{\min}$ is small. It can also be seen from (26) and (27) that shadow fading has the same impact on cumulants for the power and contention control schemes.

The accuracy evaluation of approximations under the contention control scheme is also performed and shown in Fig. 5(b). It can be seen from this figure that the log-normal approximation is fairly accurate compared to the derived interference CDFs for either pathloss-only or shadow fading channels. Moreover, it can be observed that the approximated thinning process tends to be less accurate as the CR density λ increases, which agrees with the analysis in Section III.B.

V. Imperfect Primary System Knowledge

In practice, some information about the primary system may not be perfectly known. One prominent example is the location of the primary receivers, which is usually required by CR networks in order to protect primary receivers from interfering CR transmitters. However, this information is not always available, especially in the case of passive primary receivers, i.e., when the primary receivers are hidden from CR networks. It is widely accepted that passive receiver detection techniques can be used or developed in the context of CR networks. For example, one of such primary receiver detection techniques is reported in [29]. Nevertheless, its applicability is still not convincingly viable since it requires deploying sensor nodes close to primary receivers and much coordination is involved between these sensors and CR networks as well. The most commonly used and also the simplest approach to protect the primary receiver is to regulate the transmission of the CR network based on primary transmitter sensing, assuming that primary receivers are in close proximity to the primary transmitter. In this section, we evaluate the effect of a hidden primary receiver on the resulting interference to primary receivers.

Consider a primary and CR coexisting systems depicted in Fig. 2, where an IR with radius R centered at the primary transmitter is introduced. All CR transmitters are distributed in the shaded concentric ring with inner radius R and outer radius l. Let θ be the angle between the line joining the primary transmitter (in brackets) and a CR transmitter and the line joining the primary transmitter-receiver pair (in brackets). The distance from the CR transmitter to the primary transmitter is r and the distance between the primary transmitter-receiver pair is $r_{\rm p}$. Then, the distance between the CR transmitter and the primary receiver $r_{\rm cp}$ can be expressed as

$$r_{\rm cp}(r,\theta) = \left[r^2 + r_{\rm p}^2 - 2rr_{\rm p}\cos\theta\right]^{\frac{1}{2}}, \quad r \in [R,l];\ \theta \in [0,2\pi] \tag{28}$$

where r is distributed as in (13) and θ is uniformly distributed in $[0,2\pi]$ if a Poisson point process is assumed for the CR transmitter distribution.

A. Power Control

Under the power control scheme proposed in Section II.A and the system model given in Fig. 2, the characteristic function of aggregate interference $\phi_{\rm Y}(\omega)$ can be written as follows (see Appendix D for the detailed derivation):

$$\begin{aligned}\phi_{\rm Y}(\omega) = \lim_{l\to\infty} \exp\Bigg\{ & \lambda \int_H f_{\rm h}(h) \int_0^{r_{\rm pwc}} f_{\rm cc}(x) \int_0^{2\pi}\int_R^l e^{i\omega\left(\frac{r}{r_{\rm pwc}}\right)^{\alpha} P_{\max}(x) g(r_{\rm cp}(r,\theta))h} r - r \ dr\, d\theta\, dx\, dh \\ & + \lambda \int_H f_{\rm h}(h) \int_{r_{\rm pwc}}^{\infty} f_{\rm cc}(x) \int_0^{2\pi}\int_R^l e^{i\omega P_{\max}(x) g(r_{\rm cp}(r,\theta))h} r - r \ dr\, d\theta\, dx\, dh \Bigg\}. \end{aligned} \tag{29}$$

Applying the log-normal approximation method used in Section IV, we obtain the kth cumulant of interference as

$$\begin{aligned} k_n = \lim_{l\to\infty} \lambda \Bigg\{ & \int_H f_{\rm h}(h) \int_0^{r_{\rm pwc}} f_{\rm cc}(x) \int_0^{2\pi}\int_R^l \frac{(r^{\alpha} P_{\max}(x) g(r_{\rm cp}(r,\theta))h)^n}{{r_{\rm pwc}}^{n\alpha}} r dr\, d\theta\, dx\, dh \\ & + \int_H f_{\rm h}(h) \int_{r_{\rm pwc}}^{\infty} f_{\rm cc}(x) \int_0^{2\pi}\int_R^l \left[P_{\max}(x) g(r_{\rm cp}(r,\theta))h\right]^n r dr\, d\theta\, dx\, dh \Bigg\}. \end{aligned} \tag{30}$$

As can be seen from (30), unlike (26), the kth cumulant does not have a closed-form expression. However, the complexity of obtaining the exact interference PDF from (30) is still smaller than that of the numerical method in Section III.

An experiment is done in Fig. 6(a) to examine the effect of hidden primary receiver on the resulting interference compared to the interference for the case of perfect knowledge of primary receiver location. It can be seen from the figure that the hidden primary receiver problem boosts the interference in terms of increased interference mean and variance. This figure also shows that the log-normal approximation still fits well with both the derived CDF and Monte Carlo simulations.

B. Contention Control

Under the contention control scheme proposed in Section II.B and the system model given in Fig. 2, the characteristic function of aggregate interference $\phi_Y(\omega)$ can be expressed as

$$\begin{aligned}\phi_Y(\omega) &= \lim_{l\to\infty} \exp\left\{q_{\rm mh}\lambda\pi D_l\left(E\left(e^{i\omega pg(V)h}\right)-1\right)\right\}\\ &= \lim_{l\to\infty} \exp\left\{q_{\rm mh}\lambda\pi D_l\left(\int_H f_{\rm h}(h)\int_0^{2\pi}\frac{1}{2\pi}\int_R^l \exp\left[i\omega pg(r_{\rm cp}(r,\theta))h\right]\frac{2r}{D_l}dr\,d\theta\,dh-1\right)\right\}\\ &= \lim_{l\to\infty} \exp\left\{q_{\rm mh}\lambda\int_H f_{\rm h}(h)\int_0^{2\pi}\int_R^l \exp\left[i\omega pg(r_{\rm cp}(r,\theta))h\right]r-rdr\,d\theta\,dh\right\}, \qquad (31)\end{aligned}$$

with $D_l = l^2 - R^2$.

Using the same log-normal approximation method as in Section IV, the kth cumulant of interference can be written as

$$k_n = \lim_{l\to\infty} q_{\rm mh}\lambda\int_H f_{\rm h}(h)\int_0^{2\pi}\int_R^l \left[pg(r_{\rm cp}(r,\theta))h\right]^n r - rdr\,d\theta\,dh. \qquad (32)$$

The effect of hidden primary receiver under contention control is evaluated in Fig. 6(b), where a pathloss-only channel is assumed. As we can see from this figure, the uncertainty about the primary receiver location leads to interference with larger mean and variance as compared to that in the case with perfect knowledge of primary receiver location. Moreover, it can be seen from this figure that the log-normal fitting for the interference is fairly accurate compared to the Monte Carlo simulations. The approximation approach is still applicable in this scenario.

VI. Numerical Results and Analysis

The aggregate interference power from CR transmitters employing power control or contention control is investigated numerically in this section. For the power control scheme, Fig. 7(a) shows the effect of different power control parameters on their resulting aggregate interference. The detailed setup for the initial power control scheme is as follows: the maximum transmission power for each CR transmitter $P_{\max} = 1$ W, the density of CR transmitter $\lambda = 3$ user/10^4m^2, the IR radius $R = 100$ m, the power control range $r_{\rm pwc} = 20$ m, the pathloss exponent $\beta = 4$ and the power control exponent $\alpha = 4$. From the two rightmost PDFs in this figure, it can seen that introducing power control scheme actually shifts the interference distribution leftwards compared to the distribution without power control. It means that the power control scheme can reduce the interference experienced at the primary receiver in terms of reducing its mean and slightly decreasing its variance. When deploying a CR network under the power control

scheme, its resulting interference can be controlled by manipulating several parameters including $P_{\max}$, r_{pwc}, λ, and R. It can be seen in Fig. 7(a) that the interference can be reduced by either decreasing the maximum transmission power and/or CR density, or increasing the power control range and/or IR radius. Interestingly, it also suggests that adjusting the IR radius is an effective way to control the interference, since the interference is more sensitive to the IR radius than to any other parameter as demonstrated in Fig. 7(a). Meanwhile, the interference is least sensitive to the CR user density in the sense that halving λ leads to higher interference compared to doubling r_{pwc}, halving $P_{\max}$ or doubling R.

For the contention control scheme, the impact of contention control parameters on the resulting interference is depicted in Fig. 7(b), whose initial setup is the same as that of Fig. 7(a) except that the transmission power for each CR transmitter is $p = 1$ W and the contention control range is $d_{\min} = 20$ m. It can be seen from the two rightmost PDFs in Fig. 7(b) that the contention control scheme results in an interference distribution with reduced mean like the power control scheme in Fig. 7(a). Meanwhile, the interference can be reduced by decreasing p, λ, and/or increasing R or $d_{\min}$. It can be observed by comparing Fig. 7(b) with Fig. 7(a) that (i) increasing the IR radius is an effective approach to reduce the interference for both the power and contention control schemes. However, the power control scheme is more sensitive to the IR radius than the contention control one; (ii) reducing the transmission power and/or CR transmitter density affects the interference in the very similar manner for these two control schemes.

Finally, the impact of shadow fading on the aggregate interference is investigated for different values of the Nakagami shaping factor m under power and contention control schemes, respectively, in Figs. 8(a) and 8(b). The initial setup in this example is the same as the one used for Figs. 7(a) and 7(b), except that the standard variance is $\sigma_\Omega = 4$ dB. When $m = 1$ the interfering channel becomes a Rayleigh channel, which is dominated by the log-normal shadowing. Whereas, when $m = 100$ the fluctuations of the channel are reduced significantly compared to the Rayleigh fading channel. One fact observed in Fig. 8 is that the interference distributions have larger variance and heavier tails when shadow fading is incorporated for both control schemes. Interestingly, fading tends to make the interference distribution more heavy-tailed than shadowing, i.e., the interference under shadowing has better outage property than that under fading. Moreover, the shadow fading has the similar effect for both control schemes, which agrees with the analysis in Section IV.

VII. Conclusions

Interference at a primary receiver caused by CR transmitters with different interference management mechanisms including power control, contention control, and hybrid power/contention control schemes has been characterised. The PDFs of interference for the first two mechanisms have been evaluated analytically while, the interference distribution under the hybrid power/contention control has been studied numerically. It has been found that the proposed power control and contention control schemes are two effective approaches to alleviate interference caused by CR transmitters. The hybrid control scheme causes higher interference to a primary receiver, but leads to larger CR coverage as compared to either power or contention control schemes. Then, the interference distributions for power and contention control schemes have been approximated by log-normal distributions with greatly reduced complexity using the cumulant-based approach. Furthermore, the effect of a hidden primary receiver on the perceived interference has also been investigated for the primary receiver. Numerical studies have demonstrated the impact of some CR deployment parameters on the resulting aggregate interference under power and contention control schemes. It has been shown that increasing the IR radius is an effective way to reduce the interference. Moreover, the power control scheme is more sensitive to the IR radius than the contention control counterpart. Finally, the impact of shadow fading on the aggregate interference has been analysed as well.

Acknowledgments

The authors acknowledge the support from the RCUK for the UK-China Science Bridges Project: R&D on (B)4G Wireless Mobile Communications. Z. Chen, C.-X. Wang, and J. Thompson acknowledge the support from the Scottish Funding Council for the Joint Research Institute in Signal and Image Processing between the University of Edinburgh and Heriot-Watt University, as a part of the Edinburgh Research Partnership in Engineering and Mathematics (ERPem). S. A. Vorobyov acknowledges the support in part from the Natural Sciences and Engineering Research Council (NSERC) of Canada and in part from the Alberta Ingenuity Foundation, Alberta, Canada. X. Ge acknowledges the support from National Natural Science Foundation of China (NSFC) (Grant No.: 60872007), National 863 High Technology Program of China (Grant No.: 2009AA01Z239), and the Ministry of Science and Technology (MOST) of China, International Science and Technology Collaboration Program (Grant No.: 0903). F. Zhao acknowledges the support from the NSFC (Grant No.: 60872022). C.-X. Wang and F. Zhao acknowledge the support of the Key Laboratory of Cognitive Radio and Information Processing (Guilin University of Electronic

Technology), Ministry of Education, China.

APPENDIX

A. Derivation of (15)

Substituting (6) and (7) into (14), we have

$$\begin{aligned}\phi_{\rm Y}(\omega)=&\exp\left\{\lambda\pi\int_H f_{\rm h}(h)\int_{r_{\rm cc}} f_{\rm cc}(x)\left[R^2\left(1-e^{i\omega g(R)p_{\rm pwc}(x)h}\right)+i\omega p_{\rm pwc}(x)h\int_0^{g(R)}(g^{-1}(t))^2e^{i\omega t p_{\rm pwc}(x)h}dt\right]dx\,dh\right\}\\ =&\exp\left\{\lambda\pi\int_H f_{\rm h}(h)\int_0^{r_{\rm pwc}} f_{\rm cc}(x)\left[R^2\left(1-e^{i\omega(\frac{x}{r_{\rm pwc}})^\alpha P_{\max}g(R)h}\right)+\frac{i\omega x^\alpha P_{\max}h}{r_{\rm pwc}^\alpha}\int_0^{g(R)}(g^{-1}(t))^2e^{i\omega t(\frac{x}{r_{\rm pwc}})^\alpha P_{\max}h}dt\right]dxdh\right.\\ &\left.+\lambda\pi\int_H f_{\rm h}(h)\int_{r_{\rm pwc}}^{\infty} f_{\rm cc}(x)\left[R^2\left(1-e^{i\omega g(R)P_{\max}h}\right)+i\omega P_{\max}h\int_0^{g(R)}(g^{-1}(t))^2e^{i\omega tP_{\max}h}dt\right]dx\,dh\right\}.\end{aligned} \tag{33}$$

Using (1) and (33), the characteristic function (15) is obtained.

B. Derivation of (22)

Following similar steps as in [14], the characteristic function of the aggregate interference can be expressed as

$$\phi_{\rm Y}(\omega)=\lim_{l\to\infty}e^{\lambda\pi(l^2-R^2)(Q-1)} \tag{34}$$

where

$$\begin{aligned}Q&=E\left(e^{i\omega Pg(V)H}\right)\\ &=\int_H f_{\rm h}(h)\int_R^l E\left[e^{i\omega Pg(r)h}\right]\frac{2r}{l^2-R^2}\,dr\,dh\\ &=\int_H f_{\rm h}(h)\int_R^l\left[(1-q_{\rm mh})+q_{\rm mh}e^{i\omega pg(r)h}\right]\frac{2r}{l^2-R^2}\,dr\,dh\\ &=1-q_{\rm mh}+q_{\rm mh}\int_H f_{\rm h}(h)\int_R^l e^{i\omega pg(r)h}\frac{2r}{l^2-R^2}\,dr\,dh.\end{aligned} \tag{35}$$

The integral in the last equality of (35) can be written as

$$\lim_{l\to\infty}\int_H f_{\rm h}(h)\int_R^l e^{i\omega pg(r)h}\frac{2r}{l^2-R^2}\,dr\,dh=1+\frac{1}{l^2-R^2}\int_H f_{\rm h}(h)T(\omega ph)dh \tag{36}$$

where $T(\omega ph)$ is given in (12). Substituting (35) and (36) into (34), we obtain (22).

C. Derivation of (26)

From (15) and (25), we have

$$k_n=\frac{\lambda\pi}{i^n}\int_H f_{\rm h}(h)\int_0^{r_{\rm pwc}} f_{\rm cc}(x)\left[-R^2\left(\frac{ix^\alpha P_{\max}g(R)h}{{r_{\rm pwc}}^\alpha}\right)^n+\frac{n\left(ix^\alpha P_{\max}h\right)^n}{{r_{\rm pwc}}^{n\alpha}}\int_0^{g(R)}t^{n-1-\frac{2}{\beta}}dt\right]dx\,dh$$
$$+\frac{\lambda\pi}{i^n}\int_H f_{\rm h}(h)\int_{r_{\rm pwc}}^{\infty} f_{\rm cc}(x)\left[-R^2\left(iP_{\max}g(R)h\right)^n+n\left(iP_{\max}h\right)^n\int_0^{g(R)}t^{n-1-\frac{2}{\beta}}dt\right]dx\,dh$$
$$=\lambda\pi\int_H f_{\rm h}(h)h^n dh\left(\frac{n}{n-\frac{2}{\beta}}g^{n-\frac{2}{\beta}}(R)-R^2g^n(R)\right)\left[\int_0^{r_{\rm pwc}} f_{\rm cc}(x)\frac{(x^\alpha P_{\max})^n}{{r_{\rm pwc}}^{n\alpha}}dx+\int_{r_{\rm pwc}}^{\infty} f_{\rm cc}(x)P_{\max}^n dx\right]$$
$$=\frac{2\lambda\pi P_{\max}^n}{(n\beta-2)R^{n\beta-2}}\int_H f_{\rm h}(h)h^n dh\left(\int_0^{r_{\rm pwc}}\frac{f_{\rm cc}(x)x^{n\alpha}}{{r_{\rm pwc}}^{n\alpha}}dr+\int_{r_{\rm pwc}}^{\infty} f_{\rm cc}(x)dx\right). \quad (37)$$

The first equality of (37) is obtained based on the following fact

$$\left[\frac{\partial^n}{\partial\omega^n}\right]_{\omega=0}e^{a\omega}=\left[\frac{\partial^n}{\partial\omega^n}\right]_{\omega=0}\sum_{i=0}^{\infty}\frac{(a\omega)^n}{n!}=a^n. \quad (38)$$

In the last equality of (37), the first integral can be expressed as

$$\int_H f_{\rm h}(h)h^n dh=e^{n\mu+\frac{n^2\sigma^2}{2}} \quad (39)$$

with μ and σ^2 given in (3) and (4), respectively. Also, the sum of the last two integrals in (37) can be simplified as

$$\int_0^{r_{\rm pwc}}\frac{f_{\rm cc}(x)x^{n\alpha}}{{r_{\rm pwc}}^{n\alpha}}dx+\int_{r_{\rm pwc}}^{\infty} f_{\rm cc}(x)dx$$
$$=\frac{n\alpha(n\alpha-2)\cdots 2}{{r_{\rm pwc}}^{n\alpha}(2\pi\lambda)^{\frac{n\alpha}{2}}}\left(1-e^{-\lambda\pi{r_{\rm pwc}}^2}\right)-\sum_{i=1}^{\frac{n\alpha}{2}-1}\frac{n\alpha(n\alpha-2)\cdots(n\alpha-2i+2)}{(2\pi\lambda{r_{\rm pwc}}^2)^i}{r_{\rm pwc}}^{n\alpha-2i}e^{-\lambda\pi{r_{\rm pwc}}^2}. \quad (40)$$

Substituting (39) and (40) into (37) yields (26).

D. Derivation of (29)

$$\phi_{\rm Y}(\omega)=\lim_{l\to\infty}\exp\left\{\lambda\pi D_l\left(E\left(e^{i\omega p_{\rm pwc}g(V)h}\right)-1\right)\right\}$$
$$=\lim_{l\to\infty}\exp\left\{\lambda\pi D_l\left[\int_H f_{\rm h}(h)\int_0^{\infty} f_{\rm cc}(x)\int_0^{2\pi}\frac{1}{2\pi}\int_R^l\exp\left[i\omega p_{\rm pwc}(x)g(r_{\rm cp}(r,\theta))h\right]\frac{2r}{D_l}dr\,d\theta\,dx\,dh-1\right]\right\}$$
$$=\lim_{l\to\infty}\exp\left\{\lambda\int_H f_{\rm h}(h)\int_0^{\infty} f_{\rm cc}(x)\int_0^{2\pi}\int_R^l\exp\left[i\omega p_{\rm pwc}(x)g(r_{\rm cp}(r,\theta))h\right]r-rdr\,d\theta\,dx\,dh\right\} \quad (41)$$

with $D_l=l^2-R^2$. The first equality in (41) is obtained in the same way as (34) and (35). Equation (29) can be obtained immediately from (41).

REFERENCES

[1] S. Haykin, "Cognitive radio: brain-empowered wireless communications," *IEEE J. Sel. Areas Commun.*, vol. 23, no. 2, pp. 201–220, Sept. 2005.

[2] I. F. Akyildiz, W. Y. Lee, M. C. Vuran, and S. Mohanty, "NeXt generation/dynamic spectrum access/cognitive radio wireless networks: a survey," *Computer Networks*, vol. 50, no. 13, pp. 2127–2159, Sept. 2006.

[3] Q. Zhao and B. M. Sadler, "A survey of dynamic spectrum access," *IEEE Signal Process. Mag.*, vol. 24, no. 3, pp. 79–89, May 2007.

[4] C.-X. Wang, H.-H. Chen, X. Hong, and M. Guizani, "Cognitive radio network management: tuning in to real-time conditions," *IEEE Veh. Technol. Mag.*, vol. 3, no. 1, pp. 28–35, Mar. 2008.

[5] C.-X. Wang, X. Hong, H.-H. Chen, and J. S. Thompson, "On capacity of cognitive radio networks with average interference power constraints," *IEEE Trans. Wireless Commun.*, vol. 8, no. 4, pp. 1620–1625, Apr. 2009.

[6] X. Hong, C.-X. Wang, J. Thompson, and Y. Zhang, "Demystifying white spaces," in *Proc. IEEE ICCCAS'08*, Xiamen, China, May 2008, pp. 350–354.

[7] X. Hong, C.-X. Wang, H.-H. Chen, and Y. Zhang, "Secondary spectrum access networks: recent development on the spatial models," *IEEE Veh. Technol. Mag.*, vol. 4, no. 2, pp. 36–43, June 2009.

[8] T. Kamakaris, D. Kivanc-Tureli, and U. Tureli, "Interference model for cognitive coexistence in cellular systems," in *Proc. IEEE GLOBECOM'07*, Washington DC, USA, Nov. 2007, pp. 4175–4179.

[9] R. S. Dhillon and T. X. Brown, "Models for analyzing cognitive radio interference to wireless microphones in TV bands," in *Proc. IEEE DySPAN'08*, Chicago, USA, Oct. 2008, pp. 1–10.

[10] G. L. Stuber, S. Almalfouh, and D. Sale, "Interference analysis of TV band whitespace," in *Proc. IEEE*, vol. 97, no. 4, pp. 741–754, Apr. 2009.

[11] N. Hoven and A. Sahai, "Power scaling for cognitive radio," in *Proc. IEEE WNCMC'05*, Hawaii, USA, June 2005, pp. 250–255.

[12] R. Menon, R. M. Buehrer and J. Reed, "Outage probability based comparison of underlay and overlay spectrum sharing techniques," in *Proc. IEEE DySPAN'05*, Baltimore, USA, Nov. 2005, pp. 101–109.

[13] M. Timmers, S. Pollin, A. Dejonghe, A. Bahai, L. Van der Perre, and F. Catthoor, "Accumulative interference modeling for cognitive radios with distributed channel access," in *Proc. IEEE CrownCom'08*, Singapore, May 2008, pp. 1–7.

[14] X. Hong, C.-X. Wang, and J. S. Thompson, "Interference modeling of cognitive radio networks," in *Proc. IEEE VTC'08-Spring*, Singapore, May 2008, pp. 1851–1855.

[15] R. Menon, R. Buehrer, and J. Reed, "On the impact of dynamic spectrum sharing techniques on legacy radio systems," *IEEE Trans. Wireless Commun.*, vol. 7, no. 11, pp. 4198–4207, Nov. 2008.

[16] Z. Chen, C.-X. Wang, X. Hong, J. Thompson, S. A. Vorobyov and X. Ge, "Interference modeling for cognitive radio networks with power or contention control," in *Proc. IEEE WCNC'10*, Sydney, Australia, Apr. 2010, pp. 1–6.

[17] Federal Communications Commission, "Second Report and Order and Memorandum Opinion and Order, in the matter of unlicensed operation in the TV broadcast bands (ET Docket No. 04-186) and additional spectrum for unlicensed devices below 900 MHz and in the 3 GHz band (ET Docket No. 02-380), FCC 08-260," Nov. 2008.

[18] G. L. Stuber, *Principles of Mobile Communication*, 2nd Edition, Boston: Kluwer Academic Publishers, 2001.

[19] H. Q. Nguyen, F. Baccelli and D. Kofman, "A stochastic geometry analysis of dense IEEE 802.11 networks," in *Proc. IEEE INFOCOM'07*, Anchorage, USA, May 2007, pp. 1199–1207.

[20] D. Stoyan, W. S. Kendall, and J. Mecke, *Stochastic Geometry and Its Applications*, Chichester: John Wiley & Sons, 1986.

[21] E. S. Sousa and J. A. Silvester, "Optimum transmission range in a direct-sequence spread-spectrum multihop pack radio network," *IEEE J. Sel. Areas Commun.*, vol. 8, no. 5, pp. 762–771, June 1990.

[22] X. Yang and A. P. Pertropulu, "Co-channel interference modeling and analysis in a Poisson field of interferers in wireless communications," *IEEE Trans. Signal Process.*, vol. 51, no. 1, pp. 63–76, Jan. 2003.

[23] P. C. Pinto and M. Z. Win, "Communication in a poisson field of interferers," in *Proc. IEEE 40th Annual Conf. Inform. Sciences and Systems*, Princeton, USA, Mar. 2006, pp. 432–437.

[24] J. E. Paloheimo, "On a theory of search," *Biometrika*, vol. 58, no. 1, pp. 61–75, Apr. 1971.

[25] J. Salo, L. Vuokko, H. M. El-Sallabi, and P. Vainikainen, "An additive model as a physical basis for shadow fading," *IEEE Trans. Veh. Technol.*, vol. 56, no. 1, pp. 13–26, Jan. 2007.

[26] M. Pratesi, F. Santucci, and F. Graziosi, "Generalized moment matching for the linear combination of log-normal RVs: application to outage analysis in wireless systems," *IEEE Trans. Wireless Commun.*, vol. 5, no. 5, pp. 1122–1132, May 2006.

[27] C. C. Chan and S. V. Hanly, "Calculating the outage probability in a CDMA network with spatial poisson traffic," *IEEE Trans. Veh. Technol.*, vol. 50, no. 1, pp. 183–204, Jan. 2001.

[28] R. Menon, R. M. Buehrer, and J. H. Reed, "Impact of exclusion region and spreading in spectrum-sharing ad hoc networks," in *Proc. 1st Int. Workshop on Technology and Policy for Accessing Spectrum, TAPAS'06*, Boston, USA, Aug. 2006.

[29] B. Wild and K. Ramchandran, "Detecting primary receivers for cognitive radio applications," in *Proc. IEEE DySPAN'05*, Baltimore, USA, Nov. 2005, pp. 124–130.

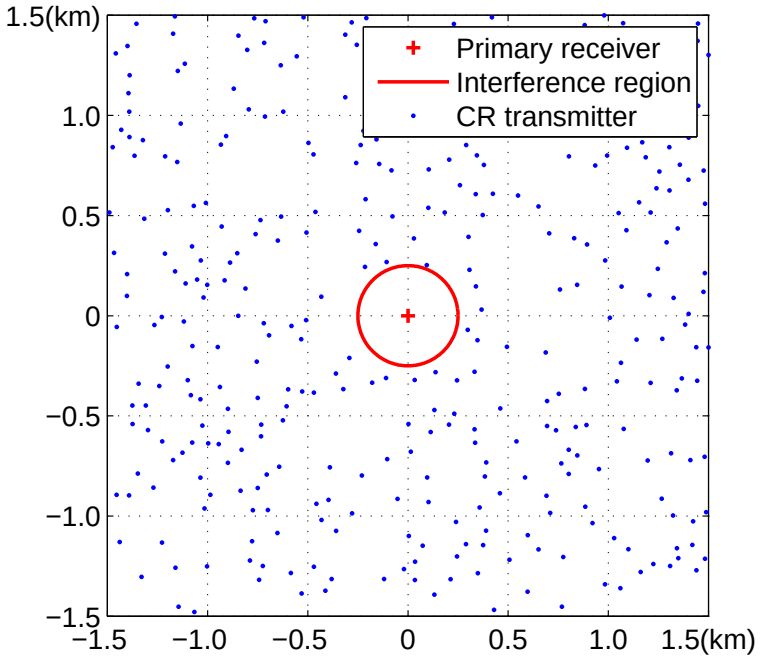

Fig. 1. System model for CR networks coexisting with a primary network ($R = 250$ m).

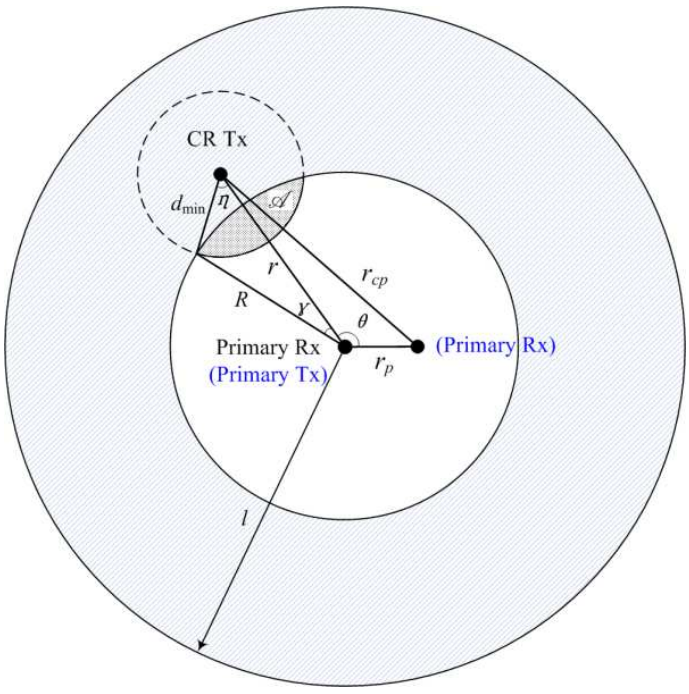

Fig. 2. Intersection of the IR and contention region (dotted region $\mathscr{A}$), and the hidden primary receiver (denoted in the bracket) which is hidden from all CR transmitters distributed in the shaded region.

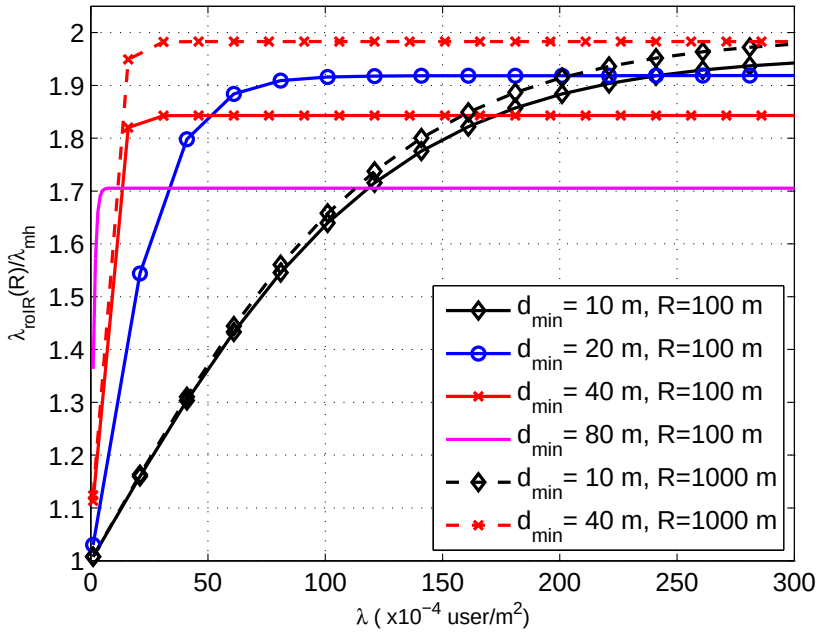

Fig. 3. Impact of system parameters on the density λ_{roIR} of active CR transmitters right outside the IR.

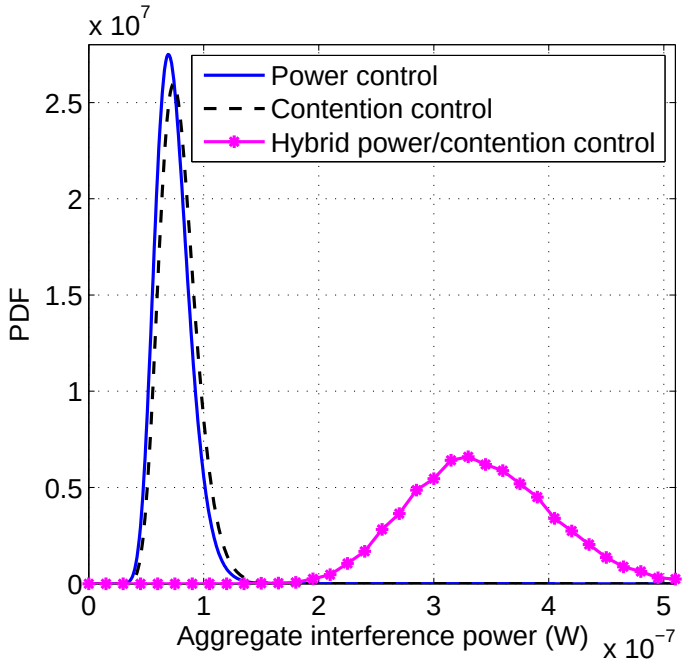

Fig. 4. Comparison of interference distributions for power, contention and hybrid power/contention control schemes (R =100 m, λ =3 user/10^{4}m^2, β =4, $r_{\mathrm{pwc}} = 20$ m, $\alpha = 4$, $P_{\max} = 1$ W, $p = 1$ W, $d_{\min} = 20$ m and $r_{\mathrm{hyb}} = 30$ m).

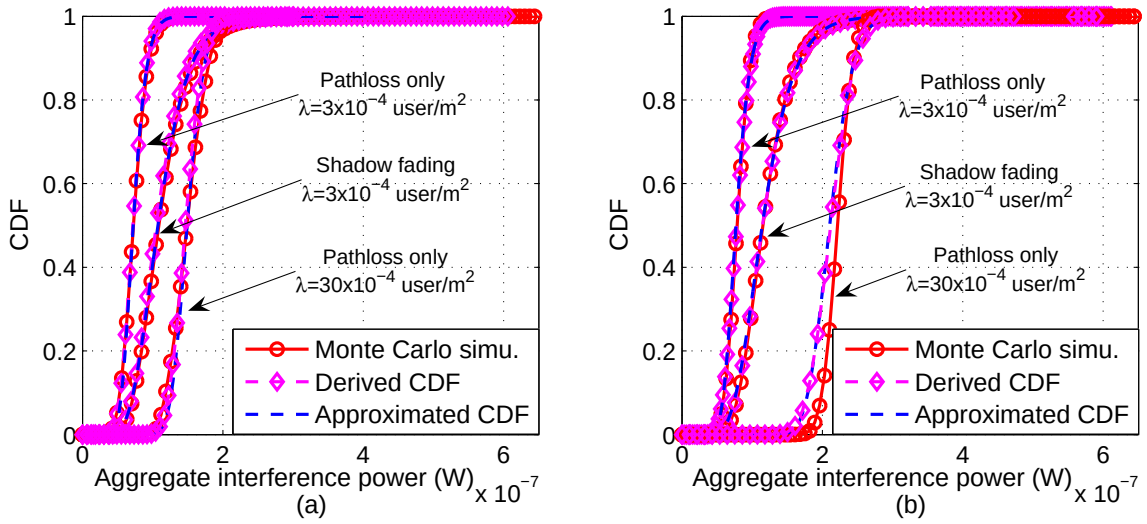

Fig. 5. Log-normal approximation for interference distribution under (a) power control (R =100 m, β =4, $r_{\rm pwc} = 20$ m, $\alpha = 4$, $P_{\max} = 1$ W, $\mu = 0$ and $\sigma = 4$ dB) or (b) contention control (R =100 m, β =4, $d_{\min} = 20$ m, $p = 1$ W, $\mu = 0$ and $\sigma = 4$ dB).

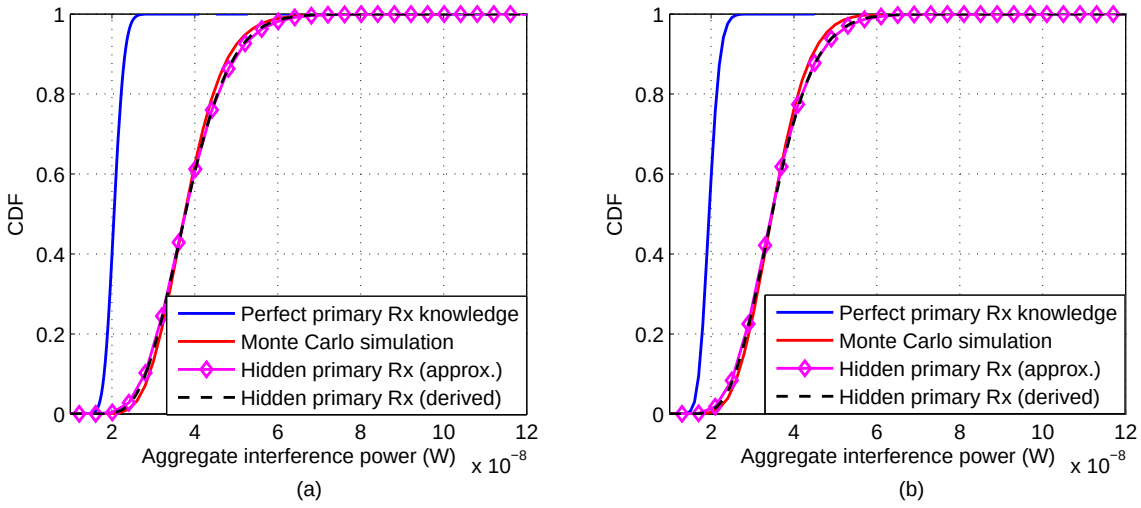

Fig. 6. Log-normal approximation for interference distribution with a hidden primary receiver under (a) power control (R =200 m, λ =3 user/10^4m^2, β =4, $r_{\rm pwc} = 20$ m, $\alpha = 4$, $P_{\max} = 1$ W and $r_p = 0.5R$) or (b) contention control (R =200 m, λ =3 user/10^4m^2, β =4, $d_{\min} = 20$ m, $p = 1$ W and $r_p = 0.5R$).

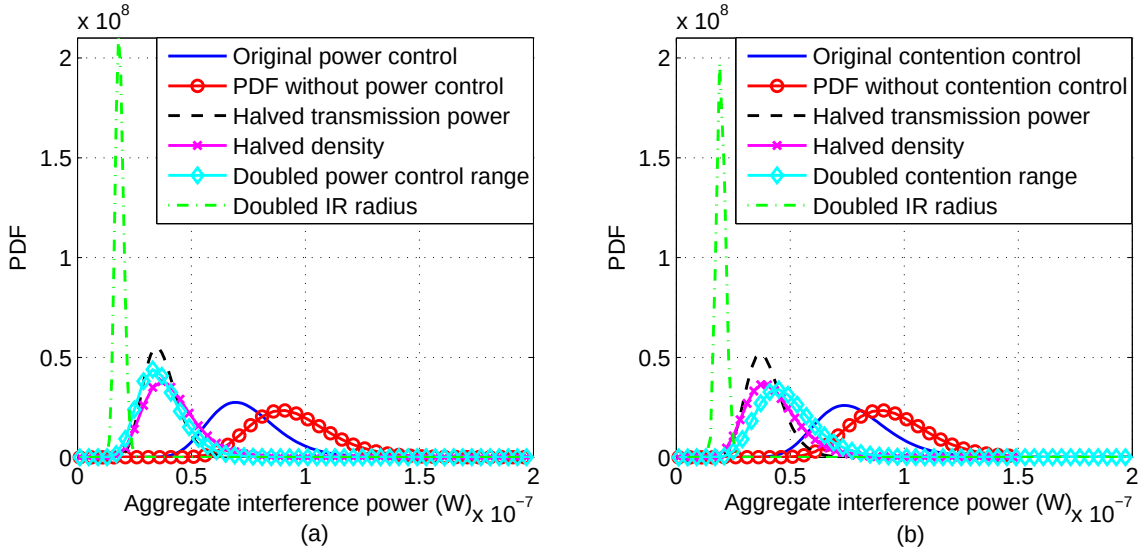

Fig. 7. Impact of various CR deployment parameters on the aggregated interference for CR networks with (a) power control (R =100 m, λ =3 user/10^4m^2, β =4, $r_{\rm pwc}$ = 20 m, $\alpha = 4$ and $P_{\max} = 1$ W) or (b) contention control (R =100 m, λ =3 user/10^4m^2, β =4, $d_{\min}$ =20 m, and $p = 1$ W).

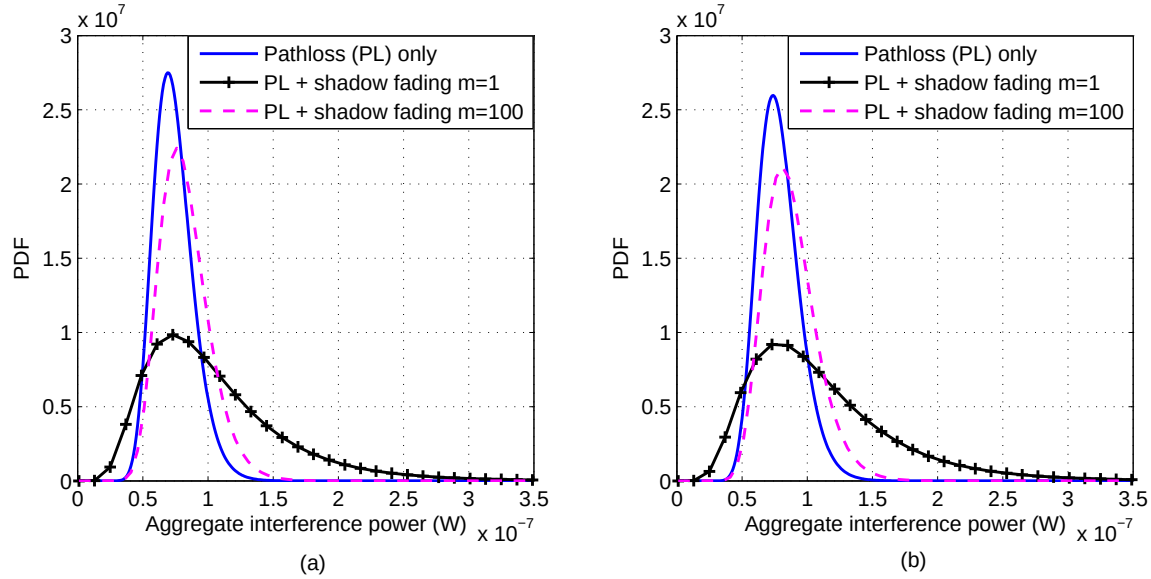

Fig. 8. Impact of shadow fading on the aggregated interference for CR networks with (a) power control (R =100 m, λ =3 user/10^4m^2, β =4, $r_{\rm pwc}$ = 20 m, $\alpha = 4$ and $P_{\max} = 1$ W) or (b) contention control (R =100 m, λ =3 user/10^4m^2, β =4, $d_{\min}$ =20 m and $p = 1$ W).